MEDICAL IMAGING

Perfusion imaging metrics after acute traumatic spinal cord injury are associated with injury severity in rats and humans

Zin Z. Khaing[1], Jannik Leyendecker[1,2], Jennifer N. Harmon[1], Sananthan Sivakanthan[1], Lindsay N. Cates[1], Jeffrey E. Hyde[1], Melissa Krueger[3], Robb W. Glenny[3], Matthew Bruce[4], Christoph P. Hofstetter[1]*

Traumatic spinal cord injury (tSCI) causes an immediate loss of neurological function, and the prediction of recovery is difficult in the acute phase. In this study, we used contrast-enhanced ultrasound imaging to quantify intraspinal vascular disruption acutely after tSCI. In a rodent thoracic tSCI model, contrast-enhanced ultrasound revealed a perfusion area deficit that was positively correlated with injury severity and negatively correlated with hindlimb locomotor function at 8 weeks after injury. The spinal perfusion index was calculated by normalizing the contrast inflow at the injury center to the contrast inflow in the injury periphery. The spinal perfusion index decreased with increasing injury severity and positively correlated with hindlimb locomotor function at 8 weeks after injury. The feasibility of intraoperative contrast-enhanced ultrasound imaging was further tested in a cohort of 27 patients with acute tSCI of varying severity and including both motor-complete and motor-incomplete tSCIs. Both the perfusion area deficit and spinal perfusion index were different between motor-complete and motor-incomplete patients. Moreover, the perfusion area deficit and spinal perfusion index correlated with the injury severity at intake and exhibited a correlation with extent of functional recovery at 6 months. Our data suggest that intraoperative contrast-enhanced, ultrasound-derived metrics are correlated with injury severity and chronic functional outcome after tSCI. Larger clinical studies are required to better assess the reliability of the proposed contrast-enhanced ultrasound biomarkers and their prognostic capacity.

INTRODUCTION

Traumatic spinal cord injury (tSCI) results in an immediate loss of neurological function, with concomitant functional, psychological, and financial consequences for both the affected individuals and their families (*1*, *2*). In the United States, more than a quarter of a million Americans are living with tSCI (*3*), and the annual incidence is 26 new cases per 100,000 individuals (*4*), resulting in estimated annual treatment costs of $9.7 billion (*5*). In clinical practice, the severity of tSCI and long-term functional outcomes are typically assessed using the International Standards for Neurological Classification of Spinal Cord Injury (ISNCSCI) at the time of the patient's presentation to the trauma hospital. This classification system provides a grading of the patient's neurological examination according to the American Spinal Injury Association (ASIA) impairment scale (AIS) (*6*, *7*). ISNCSCI is a valid, reliable, and responsive tool for assessing adults with tSCI (*8*), with several studies confirming high intrarater and interrater reliability (*9*, *10*). However, the impact of timing of the ISNCSCI examination on its predictive capacity for long-term functional outcome remains controversial (*11*). Before the adoption of contemporary spinal instrumentation at the end of the 20th century, the ISNCSCI examination was obtained upon patient transfer from acute hospitalization to an inpatient rehabilitation facility, about 1 month after tSCI, and served as a baseline for predicting long-term outcome (*12*–*15*). However, the relatively short therapeutic window of experimental neuroprotective interventions and patient desire for early prognosis have motivated the use of the ISNCSCI exam performed upon arrival at the trauma center (*16*–*18*). The need for this early marker is substantiated by the finding that spinal cord decompression within 24 hours after tSCI improves sensorimotor recovery. In contrast, surgeries conducted 24 to 36 hours after the injury are associated with a diminished neuroprotective effect of this intervention (*19*).

Several factors might contribute to the limited prognostic capacity of the ISNCSCI examination in the acute phase after injury. Even mild tSCI with subtle impingement of the spinal cord can cause transient spinal cord ischemia with temporary loss of motor and sensory function, also referred to as neurapraxia, especially in very early examinations (*20*). Consequently, ultra-early ISNCSCI examination might overestimate the injury severity as well as bias the interpretation of neuroprotective interventions (*21*, *22*). In addition, injury expansion within the first 72 hours might contribute to differences in the predictive capabilities of the ISNCSCI examination within the first 24 hours compared with 72 hours after injury. Within the first hours after tSCI, the hypoperfused injury center enlarges in both rodents and humans (*23*, *24*). Lastly, an ISNCSCI examination is impossible in patients with concomitant traumatic head injury, multisystem trauma, drug intoxication, or pharmacological sedation. In summary, several studies suggest that the prognostic capacity of the ISNCSCI examination is limited within the first 72 hours after tSCI (*22*, *25*–*27*).

Given the substantial demand for early prediction of neurological outcome, both neurochemical and imaging markers have been developed as tSCI biomarkers. Cerebral spinal fluid (CSF) collected 24 hours after tSCI contains inflammatory markers and structural proteins that accurately classify tSCI severity and predict neurological

[1]Department of Neurological Surgery, University of Washington, Seattle, WA 98105, USA. [2]University of Cologne, Faculty of Medicine and University Hospital Cologne, Department of Orthopedics and Trauma Surgery, 50937 Cologne, North Rhine-Westphalia, Germany. [3]Division of Pulmonary, Critical Care and Sleep Medicine, University of Washington, Seattle, WA 98105, USA. [4]Applied Physics Laboratory, CIMU, University of Washington, Seattle, WA 98105, USA.
*Corresponding author. Email: chh9045@uw.edu

recovery in human (*28*). However, collection of CSF requires a time-consuming lumbar puncture and laboratory analysis that are not standardized between centers. Magnetic resonance imaging (MRI) parameters, such as intramedullary lesion length, hemorrhage, and spinal cord swelling, measured on acute posttraumatic MRI have shown promise as possible predictive biomarkers (*29*–*31*). However, analyzing spinal cord parameters on MRI at the time of admission can be challenging because the spinal cord is compressed and the spinal column is misaligned.

Here, we propose ultrafast contrast-enhanced ultrasound (CEUS) as a quantitative imaging metric for acute tSCI. CEUS depicts blood flow in both the micro- and macrocirculation (*23*, *32*–*35*), the disruption of which constitutes a hallmark pathophysiological event in tSCI evolution (*36*). Our current study supports the key role of vascular disruption in the pathophysiology of tSCI. We report the development of two complementary CEUS-based parameters, the perfusion area deficit (PAD), which quantifies the amount of damaged hypoperfused spinal cord tissue, and the spinal perfusion index (SPI), which quantifies the amount of vital perfused spinal tissue at the injury center. In rodent tSCI, acutely measured PAD and SPI were correlated with injury severity and functional outcome up to 8 weeks. In a cohort of patients with tSCI, we collected perfusion-related metrics by CEUS imaging at the conclusion of early decompression and stabilization surgery (*19*). In contrast with rodent tSCI, disruption of vascular perfusion was heterogenous in our patient cohort, with both hyperperfusion and necrosis penumbra patterns detected. Our preliminary clinical data suggest that intraoperative CEUS is feasible and can provide perfusion information that may constitute a valuable indicator for assessing tSCI severity in the clinic.

RESULTS

tSCI causes disruption of spinal cord blood flow

The disruption of spinal cord parenchymal perfusion was investigated using three independent techniques: ultrafast ultrasound imaging, a microsphere deposition assay, and histological vessel patency analysis. Adult rodents underwent a moderate thoracic tSCI (150 kDyn). After tSCI, CEUS midline sagittal images were acquired. CEUS Doppler revealed disruption and displacement of intrinsic spinal cord blood vessels at the injury center (Fig. 1A). At baseline before injury in the intact spinal cord, blood volume was evenly distributed along the rostrocaudal extent of the imaged spinal cord region. Examination of blood flow changes within the microcirculation revealed a PAD centered in the injury center measuring on average 1.32 ± 0.43 mm^2 (Fig. 1A). Relative blood volume was calculated from the area under the curve (AUC) of the CEUS signal obtained during a bolus contrast injection at baseline or acutely after tSCI. Analysis of relative blood volume in rostrocaudal spinal cord segments centered on the injury site at baseline (blue) and about 30 min after a moderate tSCI (orange) showed a significant reduction in the AUC ($P < 0.0001$; Fig. 1B). Next, a microsphere deposition assay was carried out to corroborate disruption of tissue perfusion in the acutely contused spinal cord. The microsphere deposition method is a gold standard for measuring blood flow within the microcirculation. We injected microspheres before (green) and after the injury (red) (Fig. 1C) and calculated the change in perfusion as a percentage of before injury (*37*). We observed a drop in perfusion after injury within a spinal segment spanning 5 to 6 mm centered over the injury site (Fig. 1D). Tissue perfusion was disrupted in the gray matter at injury epicenter, whereas about 25% perfusion remained in the white matter (Fig. 1D). An analysis confirmed that the gray matter sustained significantly greater loss of perfusion compared with white matter after a moderate tSCI ($P < 0.05$). Intravenous infusions of lectin were used to label patent spinal cord blood vessels before and after injury in the same animal, with either red or green conjugated lectin applied before and after the injury, respectively. Analysis of lectin-labeled histology before and after injury suggested the disruption of intrinsic spinal cord blood vessels at the injury site (Fig. 1E). At the injury center, only $28.9 \pm 13.9\%$ of vessels in the gray matter remained patent compared with $54.6 \pm 17.3\%$ in the white matter (Fig. 1F). The loss of spinal cord vessel patency was most pronounced in the central gray matter and dorsal white matter tracts.

PAD is correlated with injury severity in rodent tSCI

We then studied how the injury severity influences the extent of reduced blood flow in the spinal cord parenchyma. Rodents underwent mild (100 kDyn), moderate (150 kDyn), or severe (200 kDyn) tSCI, resulting in graded degrees of hindlimb locomotor dysfunction (Fig. 2, A and B, and table S1). A degree of spontaneous locomotor and sensory recovery was detected in animals of all three severity groups, as measured by an open-field locomotor Basso, Beatie, and Bresnahan (BBB) test and ladder walk performance (Fig. 2, A and B). As expected, injury severity was related to different behavioral dysfunction during the 8-week postinjury (wpi) period in all animals (Fig. 2, A and B).

CEUS was performed acutely after tSCI to evaluate perfusion and directional blood flow in the spinal cord (Fig. 2C). The PAD was 0.41 ± 0.10, 1.32 ± 0.43, and 2.87 ± 0.27 mm^2 in mild, moderate, and severe rodent tSCI, respectively ($P < 0.001$; Fig. 2D). The extent of the PAD increased with injury severity in both the rostrocaudal and dorsoventral directions (Fig. 2D). The PAD size measured on acute CEUS was significantly correlated with BBB scores at both 2 and 8 wpi ($r^2 = 0.80$, $P < 0.0001$ and $r^2 = 0.82$, $P < 0.001$, respectively; Fig. 2E and fig. S1A). PAD was also significantly positively correlated with 2- and 8-wpi ladder walk missed steps ($r^2 = 0.60$, $P < 0.01$ and $r^2 = 0.65$, $P < 0.001$, respectively; Fig. 2F and fig. S1B). PAD was negatively correlated with the extent of spared myelin at the epicenter, as determined by a histological analysis 8 wpi ($r^2 = 0.72$, $P < 0.001$; fig. S1C). Combined, these data suggest that, acutely after tSCI, PAD is associated with metrics of chronic functional deficits in rodent tSCI.

SPI correlates with functional outcome in rodent tSCI

We quantified the residual perfused spinal cord parenchyma at the injury center relative to the uninjured portion of the spinal cord as a possible surrogate for vital tissue. We developed this index of spinal perfusion as the contrast inflow in the injury center normalized to the contrast inflow in the spinal cord parenchyma rostral and caudal to the injury (Fig. 3A). The SPI was calculated in all CEUS obtained acutely after rodent tSCI. The SPI measured 0.89 ± 0.04, 0.51 ± 0.11, and 0.34 ± 0.06 in mild (100 kDyn), moderate (150 kDyn), and severe (200 kDyn) rodent tSCI, respectively (Fig. 3B). The SPI in mild tSCI was significantly higher compared with moderate ($P < 0.05$) and with severe tSCI ($P < 0.001$) (Fig. 3B). Acute CEUS SPI exhibited a significant correlation with hindlimb locomotor deficit graded

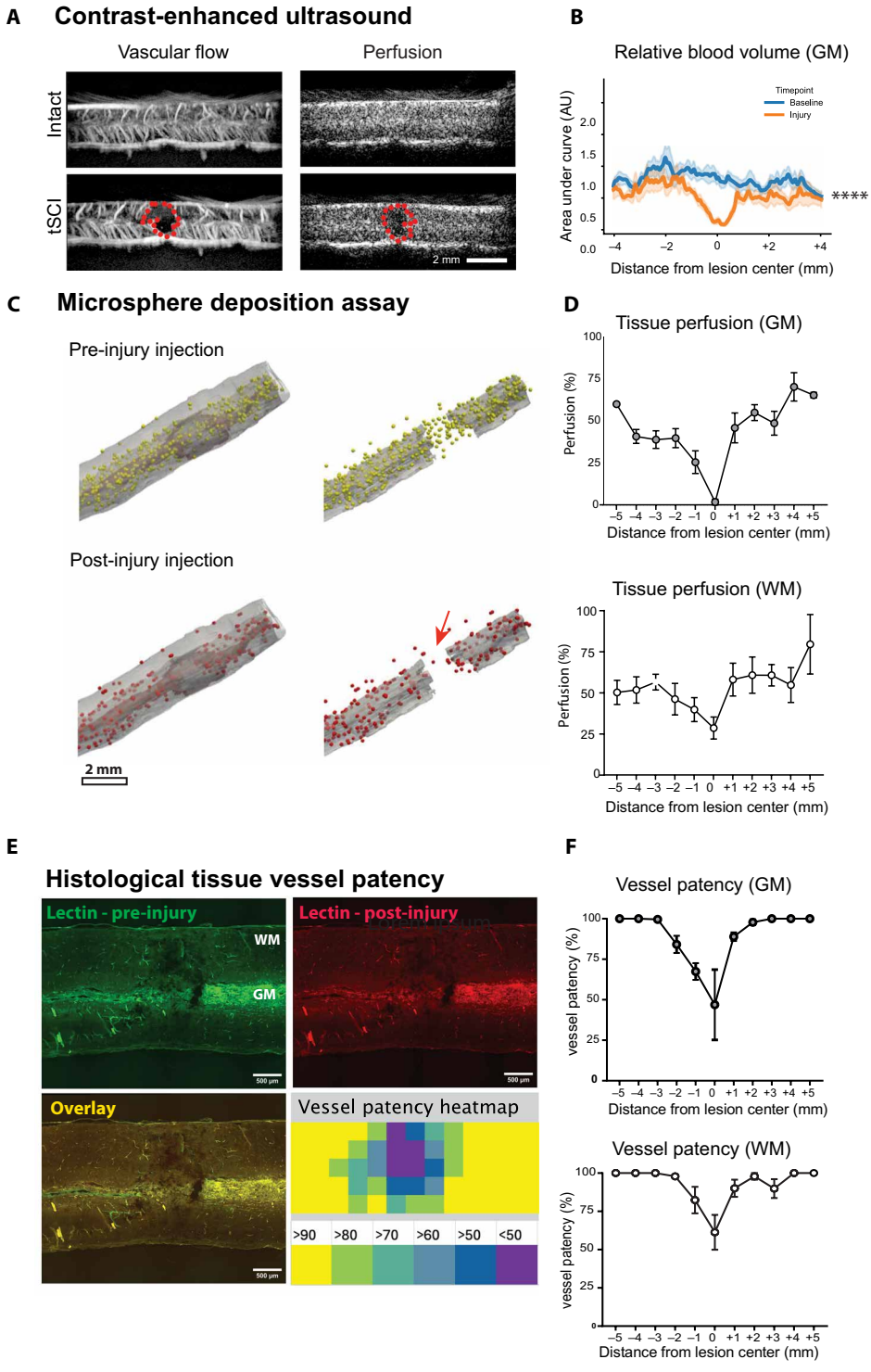

Fig. 1. tSCI causes disruption of spinal cord blood flow and perfusion. (**A**) Representative CEUS midline sagittal images of the thoracic rat spinal cord. Red dotted line, injury center. Scale bar, 2 mm. (**B**) Analysis of relative blood volume in the gray matter (GM) estimated by the AUC in rostrocaudal spinal cord segments centered on the injury center at baseline (blue) and at about 30 min after a 150-kDyn injury (orange). AU, arbitrary units. Data are presented as means ± SD; two-way ANOVA followed by lesion status and location followed by Bonferroni's multiple comparisons test. $P < 0.0001$; $n = 6$. (**C**) Representative microsphere deposition renderings in a rat spinal cord with injection before injury (yellow) and after injury (red). Dots represent individual florescent microspheres detected within the spinal cord. Light gray, white matter (WM); dark gray, GM. Red arrow, injury epicenter. Scale bar, 2 mm. (**D**) Quantification of gray (top) and white (bottom) matter percent change in perfusion from preinjury in microsphere deposition assay relative to distance from the center of a 150-kDyn tSCI lesion. Data are presented as means ± SEM. $n = 9$. (**E**) Representative histological images of spinal cord lectin vascular labeling before and after tSCI in rat. Green, preinjury lectin injection; red, postinjury lectin injection. Scale bars, 500 μm. Heatmap of vessel patency. Color scale, % patency. $n = 6$. (**F**) Quantification of vessel patency at the injury site in gray (top) and white (bottom) matter. Data are presented as means ± SEM. $n = 6$.

by BBB testing at both 2 and 8 wpi ($r^2 = 0.84$, $P < 0.0001$ and $r^2 = 0.83$, $P < 0.001$, respectively; Fig. 3C and fig. S2A). Similarly, the SPI was correlated with the number of missed steps in the ladder walk at 2 and 8 wpi ($r^2 = 0.71$, $P < 0.0001$ and $r^2 = 0.58$, $P < 0.01$, respectively Fig. 3D and fig. S2B), and the amount of spared myelin at the epicenter at 8 wpi ($r^2 = 0.68$, $P < 0.01$; fig. S3). SPI was also correlated with the PAD ($r^2 = 0.90$, $P < 0.001$; Fig. 3E).

CEUS analysis of PAD and SPI is feasible in patients with acute tSCI

To evaluate the feasibility of acquiring PAD and SPI in patients with acute tSCI and to investigate their relationship with recovery metrics in human, we enrolled a total of 27 patients with acute tSCI who underwent posterior surgical spinal decompression and stabilization. The cohort was, on average, 55.1 ± 4.1 years old and consisted

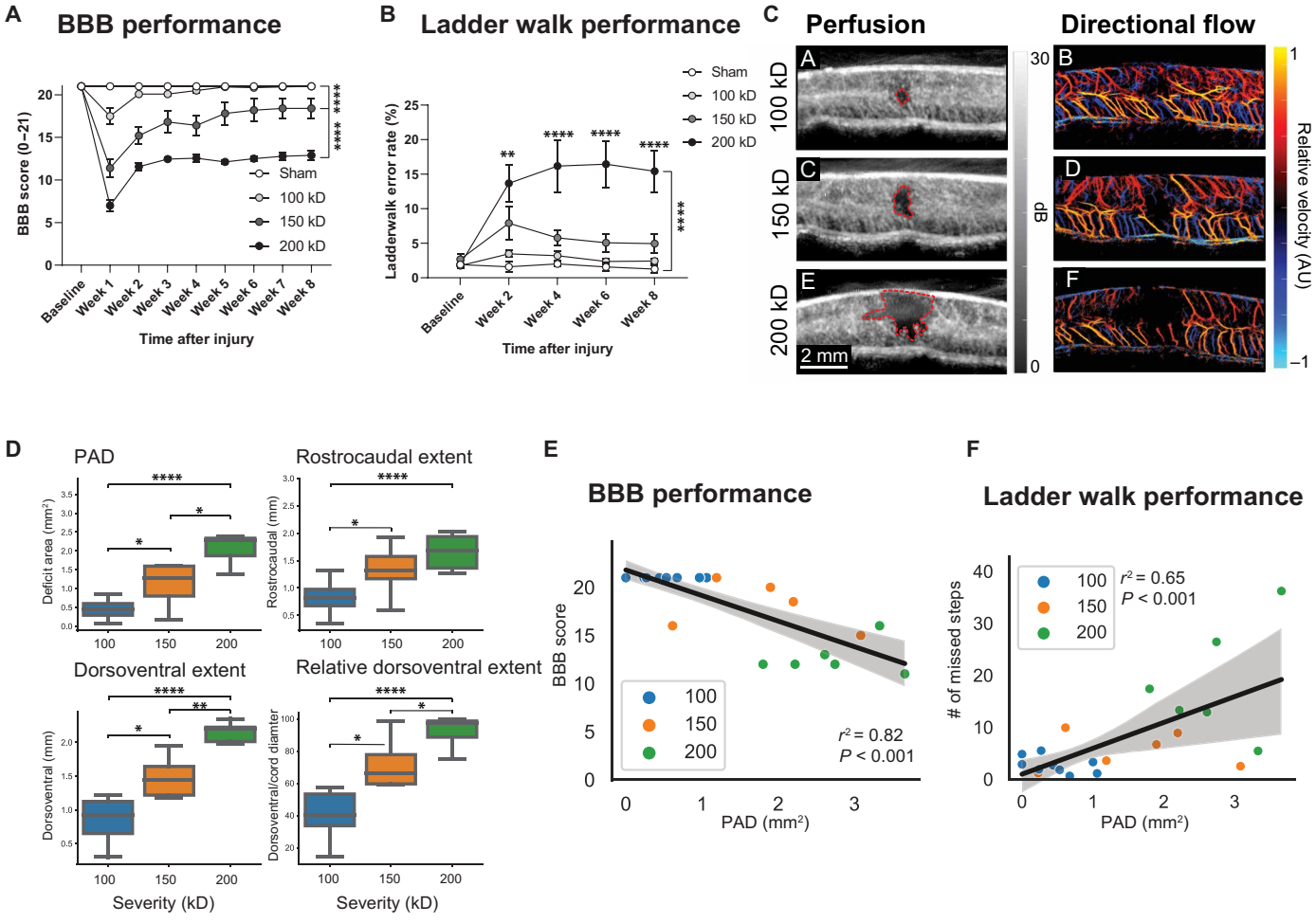

Fig. 2. PAD is correlated with functional outcome in rodent tSCI. (**A** and **B**) Behavioral assessments using BBB (A) and ladder walk (B) testing. kD, kDyn. Data are presented as means ± SEM. Analysis by two-way ANOVA, followed by Tukey's post hoc test. $^{**}P < 0.01$ and $^{****}P < 0.0001$. $n = 4$, sham; $n = 10$, 100 kDyn; $n = 6$, 150 kDyn; and $n = 6$, 200 kDyn. (**C**) Representative images of rodent spinal cord by ultrafast CEUS Doppler tissue perfusion (left; red dotted line, PAD; gray scale, dB) and super-resolution ultrasound localization imaging depicting directional flow [right; color scale, relative velocity (AU); red, toward dorsal flow; blue, toward ventral flow]. Scale bar, 2 mm. (**D**) Analysis of PAD, rostrocaudal, dorsoventral, and relative dorsoventral dimensions of PAD. Data are presented as box plots with minimum, maximum, median, and quartiles. Analysis by one-way ANOVA for lesion severity followed by Tukey's post hoc test. $^{*}P < 0.05$, $^{***}P < 0.01$, and $^{****}P < 0.0001$. (**E** and **F**) Correlation analysis of acute PAD and BBB hindlimb locomotor test (E) or PAD and missed steps in the ladder walk test (F). Each data point represents an individual animal. Pearson's correlation analysis, $r^2 = 0.82$, $P < 0.001$ (E), and r^2 0.65, $P < 0.001$ (F). [(C) to (F)] 100 kDyn, $n = 10$; 150 kDyn, $n = 6$; and 200 kDyn, $n = 6$.

of 5 female and 22 male patients. The cause of tSCI was motor vehicle accidents ($n = 13$, 48.2%), falls from height ($n = 9$, 33.3%), and falls from ground ($n = 5$, 18.5%). The injury locations were in the cervical spine ($n = 22$, 81.5%) and the thoracic spine ($n = 5$, 18.5%) (table S2). At the time of admission, to assess acute neurological impairment, we evaluated and graded each participant by AIS grade. Complete motor and sensory loss (AIS grade A) was documented in 14 patients (51.9%), whereas the remaining 13 patients suffered from incomplete tSCI (AIS grade C, $n = 9$, 33.3%; AIS grade D, $n = 4$, 14.8%) (table S2). All patients underwent posterior surgical decompression and fusion followed by intraoperative CEUS, on average, 16.6 ± 2.5 hours after the traumatic event. Stabilizing pedicle screw-rod construct involved, on average, 5.6 ± 0.3 spinal segments and spanned the cervicothoracic junction in 16 (59.3%) patients. All patients underwent direct decompression of the contused spinal cord by having, on average, 3.0 ± 0.3 laminae removed. The estimated blood loss was 479.6 ± 86.9 ml. Surgeries took, on average, 211.1 ± 13.3 min to complete (table S3).

Before closing the surgical wound, all patients underwent ultrasound imaging of the injured spinal cord. Ultrasound B-mode images revealed hyperechogenicity, consistent with hemorrhagic contusion, at the site of tSCI in all patients (Fig. 4A). In motor-incomplete tSCIs, hyperechogenicity was typically confined to the central gray matter, whereas more extensive pathological changes were seen in motor-complete injuries. An intravenous bolus of contrast agent was given, and contrast inflow was recorded on sagittal midline CEUS. During the time of CEUS acquisition, 92.6% of patients required pressure support to maintain mean arterial blood pressures at 81.3 ± 1.4 mmHg. Surgeries and CEUS were well tolerated. We did not encounter any intraoperative complications associated with surgeries or CEUS imaging. Three patients in our cohort passed away during the initial hospitalization, and an additional two patients succumbed to

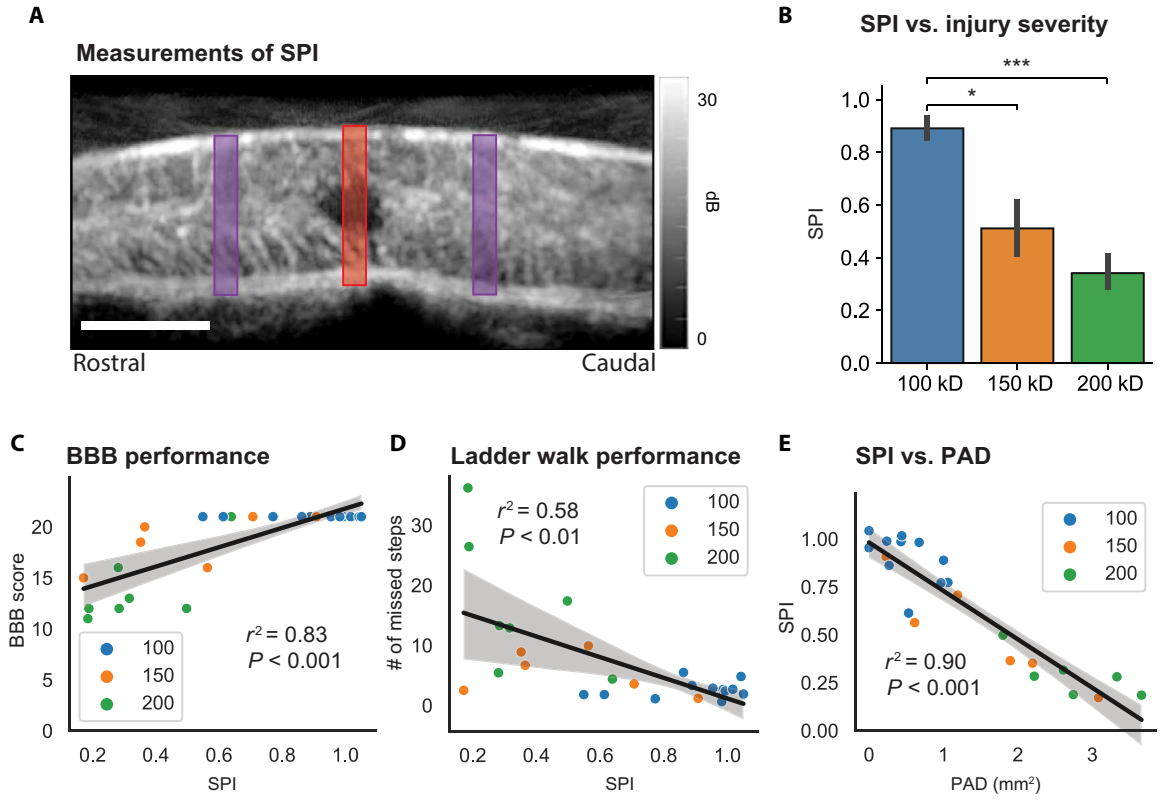

Fig. 3. SPI is correlated with injury severity and functional outcome in rodent tSCI. (**A**) Representative CEUS image of rodent spinal cord with SPI ROIs overlaid. Injury, red; reference, purple. Scale bar, 2 mm. (**B**) Normalized SPI in 100-, 150-, or 200-kDyn rodent tSCI. Data are presented as means ± SEM. Analysis by one-way ANOVA followed by Tukey's post hoc test. *$P < 0.05$ and ***$P < 0.001$. (**C**) Relationship of acute SPI and the hindlimb BBB locomotor score 8 wpi. Pearson's correlation analysis, $r^2 = 0.83$, $P < 0.001$. (**D**) The relationship of acute SPI and the number of missed steps during ladder walk testing 8 wpi. Pearson's correlation analysis, $r^2 = 0.58$, $P < 0.01$. (**E**) Relationship of acute SPI and PAD in the rodent tSCI model. Pearson's correlation analysis, $r^2 = 0.90$, $P < 0.001$. 100 kDyn, $n = 10$; 150 kDyn, $n = 6$; and 200 kDyn, $n = 6$.

tSCI-related complications within the 6-month follow-up period. All patients underwent a complete ISNCSCI examination before the surgery upon admission to Harborview emergency room, and 22 patients completed the exam again 6 months after their injury.

Analysis of contrast inflow on sagittal ultrasound studies revealed a PAD in 21 (77.8%) patients (Fig. 4A). All patients lacking discernible PAD were individuals with incomplete tSCI and were graded as either AIS C or D at admission. There was no statistically significant correlation between PAD and T2-hyperintense intramedullary edema on preoperative MRI in a subset of the cohort ($n = 17$; $r^2 = 0.32$, $P > 0.05$; fig. S4A). PAD was positively correlated with the AIS grade determined at admission ($r_s = 0.83$, $P < 0.01$; fig. S4B). Patients with incomplete tSCI had a significantly smaller PAD compared with those with complete tSCI (8.3 ± 3.8 mm^2 versus 89.4 ± 11.8 mm^2; $P < 0.001$; Fig. 4B). A total of 16 patients (57.1%) showed improvement in their AIS grades at the last available follow-up examination compared with their initial assessment (Table 1). Functional improvement was observed in just 35.7% of patients with AIS A, whereas improvement was more frequently seen in those with AIS C and D (77.8 and 100%, respectively). Patients who experienced functional improvement had a significantly smaller PAD compared with patients who did not exhibit AIS grade improvement (20.8 ± 7.8 versus 86.1 ± 15.5, $P < 0.001$; fig. S4C). The size of the PAD measured on acute intraoperative CEUS exhibited a positive correlation with the 6-month AIS injury severity ($r_s = 0.83$, $P < 0.001$; Fig. 4C). Receiver operating characteristic (ROC) analysis revealed that a PAD cutoff of 53.2 mm^2 was related to the AIS grade of the spinal cord injury with an AUC of 0.98 ($P < 0.001$; Fig. 4D).

We then quantified the amount of perfused spinal cord tissue at the injury center by calculating the SPI (Fig. 5A). In contrast to rodent tSCI, patients with mild tSCI (AIS D) had pronounced hyperemia at the site of injury as evidenced by an average SPI of 1.7 ± 0.37. All hyperemic tSCI lesions were detected in patients with cervical tSCI. The intraoperative SPI exhibited a significant negative correlation with injury severity as determine by the ISNCSCI examination at admission ($r_s = 0.77$, $P < 0.001$; fig. S4D). Patients with complete tSCI at admission had an SPI that was significantly smaller compared with patients with incomplete tSCI (0.37 ± 0.11 versus 1.48 ± 0.13; $P < 0.001$; Fig. 5B). SPI exhibited a negative correlation with the AIS score at last follow-up ($r_s = -0.82$, $P < 0.001$; Fig. 5C). Patients with an improved AIS grade at the time of their last follow-up had a significantly higher SPI compared with patients who did not exhibit AIS score improvement (1.28 ± 0.15 versus 0.45 ± 0.18, $P < 0.001$; fig. S4E). ROC analysis revealed that a SPI cutoff of 0.57 was associated with completeness of the spinal cord injury with an AUC of 0.96 ($P < 0.001$; Fig. 5D). Last, compared with our rodent tSCI model, SPI and PAD in our patient cohort exhibited a less strong albeit statistically significant correlation ($r^2 = 0.73$, $P < 0.001$; Fig. 5E).

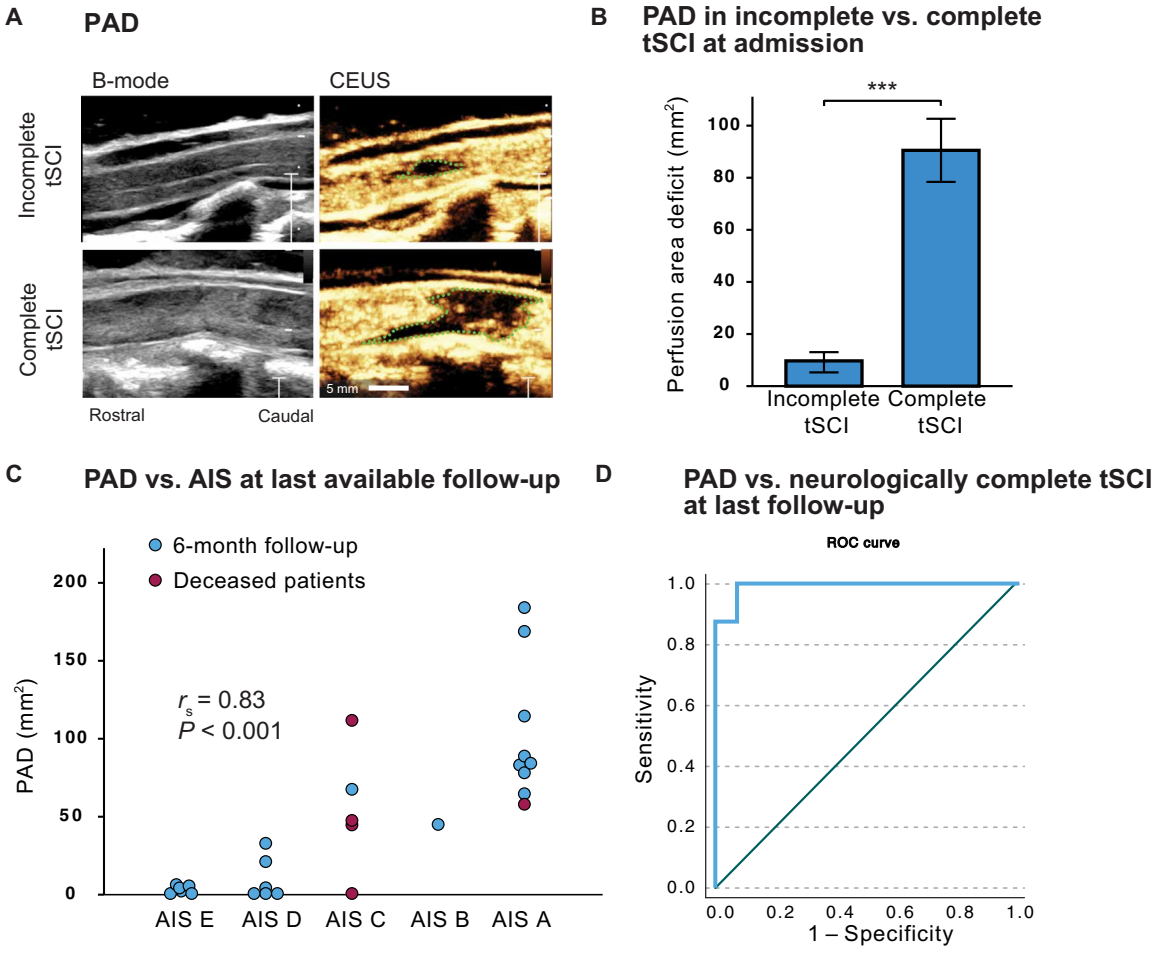

Fig. 4. PAD is related to injury severity in human tSCI. (**A**) Representative intraoperative ultrasound displaying B-mode (left) and tissue perfusion (right) images after surgical decompression of a motor-incomplete (top row) and motor-complete (bottom row) human tSCI. Green dotted line, PAD. Scale bar, 5 mm. (**B**) Comparison of PAD area between participants with admission exam motor-incomplete (AIS C to E) or motor-complete (AIS A and B). Data are presented as means ± SEM. Mann-Whitney *U* test, ***$P < 0.001$. Incomplete tSCI: $n = 13$; complete tSCI: $n = 14$. (**C**) Scatterplot of PAD in patients with acute tSCI in relation to the AIS grade at 6 months or last available follow-up Spearman's rank correlation analysis, $r_s = 0.83$, $P < 0.001$. AIS E, $n = 6$; AIS D, $n = 6$; AIS C, $n = 5$; AIS B, $n = 1$; AIS A, $n = 9$. (**D**) ROC of PAD versus completeness of tSCI at the last follow-up. AUC = 0.98 ($P < 0.001$; $n = 22$).

Table 1. Patient neurological outcomes. Data are presented as number of participants (% of cohort). $n = 27$.

AIS grade admission	*N* (% of total)	AIS grade improvement (% of grade)	Mortality (% of grade)
A	14 (51.9%)	5 (35.7%)	3 (21.4%)
B	0	0	0
C	9 (33.3%)	7 (77.8%)	2 (22.2%)
D	4 (14.8%)	4 (100%)	0 (0.0%)

DISCUSSION

In this study, we introduce CEUS-derived metrics to quantify damaged spinal cord tissue (PAD) and residual perfused tissue (SPI) in acute tSCI. In rodent models, acute CEUS-derived PAD and SPI correlate with injury severity and functional outcomes. We also demonstrate the feasibility and safety of acquiring and calculating CEUS-derived metrics intraoperatively in patients with acute tSCI. CEUS in human tSCI reveals distinct patterns of vascular disruption and promising prognostic potential.

We used CEUS to evaluate vascular disruption, a critical initial pathophysiological event after tSCI (*36*). Disruption of spinal cord blood flow with subsequent ischemia has been documented in a variety of tSCI models using different techniques, such as microangiography (*38*, *39*), autoradiography (*40*, *41*), hydrogen electrode

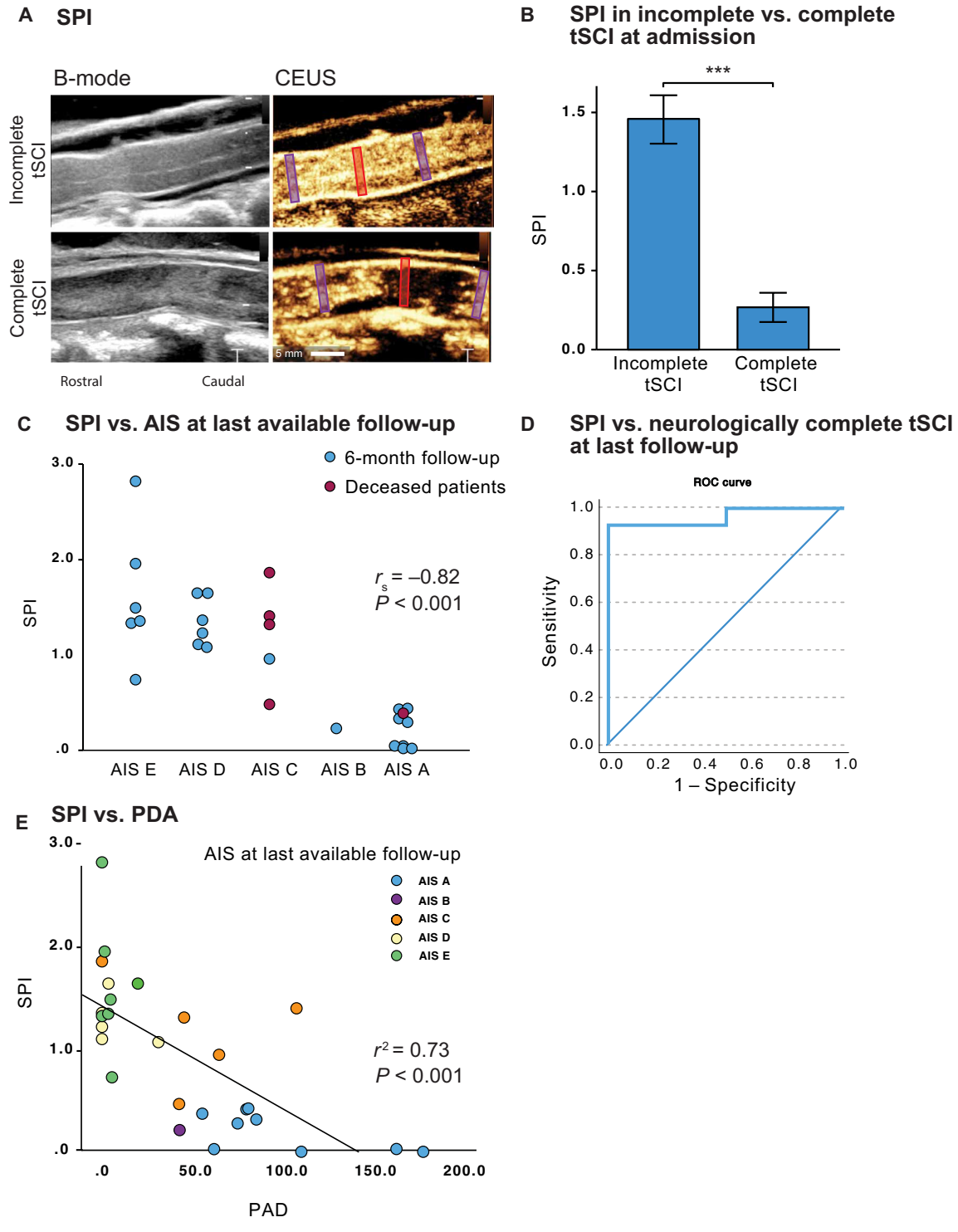

Fig. 5. SPI is related to injury severity in human tSCI. (**A**) Representative intraoperative ultrasound of B-mode (left) and tissue perfusion (right) in motor-incomplete (top row) and motor-complete (bottom row) human tSCI. Injury center, red; rostral and caudal reference regions, purple. (**B**) SPI of patients with motor-incomplete (AIS C to E) and motor-complete (AIS A and B) determined on admission exam. Data are presented as means ± SEM; Mann-Whitney *U* test, ***$P < 0.001$. Incomplete tSCI, $n = 13$; complete tSCI, $n = 14$. (**C**) Intraoperative SPI in relation to AIS grade at the last available follow-up. Spearman's rank correlation analysis, $r_s = –0.82$, $P < 0.001$. AIS E, $n = 6$; AIS D, $n = 6$; AIS C, $n = 5$; AIS B, $n = 1$; AIS A, $n = 9$. (**D**) ROC of SPI versus completeness of tSCI at the last follow-up. AUC = 0.96 ($P < 0.001$; $n = 22$). (**E**) Scatterplot of the relationship between SPI and PAD in the patient cohort. Pearson's correlation analysis, $r^2 = 0.73$, $P < 0.001$; $n = 27$.

(*42*), and the microsphere deposition assay (*39*). In the current report, we corroborate the disruption of spinal cord perfusion in rodent tSCI models of varying severity using two gold-standard methods, the fluorescent microspheres deposition assay and vessel patency using histological methods. Several studies have demonstrated that the degree of vascular disruption is directly proportional to the severity of tSCI. A linear relationship between tSCI severity and spinal cord blood flow at the injury site has been demonstrated (*43*). In these experiments, adult rats were subjected to mild, moderate, or severe cervical compression tSCI, and spinal cord blood flow was measured using the hydrogen clearance technique 30 min after injury. Our laboratory recently corroborated an injury severity–dependent decrease of spinal cord perfusion in rodents using CEUS (*35*). A severe contusion tSCI in the thoracic spinal cord resulted in a substantially larger PAD compared with a moderate tSCI. PAD correlated with the hindlimb locomotor score at 8 wpi. In the current study, we demonstrated that the size of the PAD is correlated with injury severity, underscoring the close link between vascular disruption and the severity of injury in rodent and human tSCI.

The human patient cohort exhibited heterogeneity in tSCI severity, injury location, and etiology, which aligns with existing literature (*44*). Consequently, the size of the PAD in patients was more variable than in the controlled rodent injury model (*45*). In some patients with motor-incomplete injuries, PAD was minimal or absent. Additional variability in the human cohort included factors such as age, comorbidities, and preexisting spinal conditions, such as myelopathy, stenosis, or prior surgeries. Low-energy trauma, such as ground falls, can injure the spinal cord, especially when it is confined in a stenotic spinal canal, such as in central cord syndrome (*46*). Given the aging of our society, the incidence of central cord syndrome is rising rapidly (*47*). In addition, high-energy trauma, such as high-speed car accidents, may cause disruption of the spinal column with violent contusion, stretch, or disruption of the spinal cord. Previous studies using intraoperative laser speckle imaging after acute tSCI demonstrated three distinct pathological patterns of spinal cord blood flow: a necrosis-penumbra pattern (observed in thoracic injuries), a hyperperfusion pattern (observed in cervical injuries), and a patchy-perfusion pattern (found in cervical and thoracic injuries) (*48*). In our study, we detected both the necrosis-penumbra and hyperperfusion patterns using CEUS. The patchy-perfusion pattern was not observed in our study, which may be due to our limited patient cohort or the fact that this particular perfusion pattern is restricted to superficial spinal cord tissue, whereas CEUS visualizes the entire diameter of the spinal cord.

In our patient cohort, we detected increased tissue perfusion at the injury center compared with the spared periphery in patients with incomplete cervical tSCI. Posttraumatic tissue hyperemia is a complex physiological response involving various mechanisms that have been studied across several organ systems. Increases in inflammatory cytokines, tissue catabolism, and hypoxia are associated with an acute rise in blood flow to traumatized tissue (*49*, *50*). There is a paucity of data regarding posttraumatic hyperperfusion in the spinal cord. Our study found that the hyperperfusion pattern is typically observed in patients with cervical tSCI, consistent with the existing literature (*48*). Moreover, our data suggest that hyperperfusion may be associated with less severe motor-incomplete tSCI. This aligns with a preclinical study, where hyperemia was observed after transient (1 hour or less) nondestructive loading of the canine spinal cord (*51*). However, in our patient cohort, we did not detect a correlation between SPI and the interval between injury and surgical decompression. Moreover, the SPI did not exhibit a detectable correlation with the mean arterial pressure at the time of acquisition in our patient cohort ($n = 27$, $r^2 = 0.1$; $P = 0.138$). Note that in rat studies, the spinal cord was exposed before injury and in patients after injury, and the bony decompression itself may influence the hemodynamic patterns, such as hyperemia, observed in humans. The impact of various posttraumatic perfusion patterns on injury evolution and recovery is an intriguing topic for future studies.

We propose that CEUS-derived PAD may be a surrogate measure for damaged spinal cord parenchyma. Almost all prognostic biomarkers for tSCI are either directly or indirectly related to the amount of damaged spinal parenchyma. Cerebrospinal fluid and serum biomarkers comprise cellular proteins discharged from structurally damaged cells into the subarachnoid space or bloodstream. The magnitude of structural spinal cord damage correlates with injury severity and potentially the clinical outcome (*52*). Among various markers, inflammatory, autoimmune, neuronal, and astroglia markers have demonstrated promising predictive capacity in human trials (*28*). Elevated posttraumatic cerebrospinal fluid concentrations of cytokines such as interleukin-6 (IL-6) and IL-8, as well as glial fibrillary acidic protein (GFAP) correlate with AIS grades. Protein concentrations of IL-6, IL-8, monocyte chemoattractant protein-1 (MCP-1), tau, S100b, and GFAP are associated with neurological recovery, with reduced concentrations observed in patients showing improvement (*53*). In addition, phosphorylated neurofilament heavy chain (pNF-H) and neuron-specific enolase (NSE) serve diagnostic purposes, because serum or CSF concentrations reflect injury severity with elevated concentrations observed 24 and 48 hours after the injury (*54*, *55*). Furthermore, prolonged pNF-H elevations 48 hours after the injury are associated with higher mortality. However, the use of serum and CSF biomarkers in the context of spinal cord injuries faces substantial limitations. First, the practical application of these markers can be hampered by the need for sample acquisition, especially in the case of CSF, which necessitates labor-intensive lumbar puncture procedures. In addition, these biomarkers require time to reach elevated concentrations after tSCI, limiting their use in acutely sampled CSF and potentially delaying diagnosis and intervention. Moreover, the variability in sample processing times and the need for standardized laboratory protocols can introduce challenges in achieving consistent and reliable results.

MRI-based measurements represent another type of prognostic imaging biomarker for tSCI. An array of sequences has successfully predicted the probability of short-term improvements after tSCI. In T2-weighted MRI scans, the sagittal intramedullary lesion length, intramedullary hemorrhage, and spinal cord signal abnormalities demonstrate a strong correlation with the extent of neurologic impairment and functional conversion (*29*, *30*, *56*). In addition, MRI abnormalities both rostral and caudal to the lesion and in the cerebral cortex correspond with functional outcomes, suggesting both anterograde and retrograde posttraumatic degeneration (*57*–*60*). MRI has also been used to examine the properties of traumatized spinal cord parenchyma. The use of diffusion tensor imaging (DTI) MRI offers a promising method to assess white matter pathology in tSCI (*61*, *62*). DTI analyzes the speed and direction of water diffusion to assess fiber tract microstructure and anatomy and is feasible in human tSCI (*63*). However, the use of MRI biomarkers in spinal

cord injuries faces substantial limitations. First, the correlation of MRI-based fiber tractography with neurological impairments has only been demonstrated in chronic tSCI (*64*). DTI obtained acutely after tSCI lacks prognostic capacity because potentially preserved white matter tracts are compressed and distorted by the disrupted spinal column (*65*). Second, the spatial resolution of MRI may be inadequate for capturing fine structural changes that indicate tissue damage. Third, not all patients with acute tSCI undergo MRI for various reasons, including the unavailability of MRI during off hours, the limited value of MRI for treatment decisions, or the patients being hemodynamically unstable. At our level 1 trauma center, only about 50% of tSCI patients undergo preoperative MRI. These challenges underscore the urgent need to develop alternative diagnostic imaging methods.

We advocate for the incorporation of CEUS as an imaging modality for evaluating acute tSCI. This technology offers a host of advantages compared with other imaging techniques, including spatial resolution of less than 1 mm, which enables precise characterization of the injury extent and identification of areas with perfused vital spinal cord parenchyma. Real-time ultrasound imaging provides surgeons with real-time dynamic physiological information, supporting the evaluation for additional surgical maneuvers (such as additional resection of bone fragments) in about one-third of our patients. Of particular importance is the technology's ability to assess perfused tissue at the injury site intraoperatively. Vital, perfused spinal cord tissue is the target of neuroprotective interventions and serves as a predictor of functional outcomes.

Our study is not without limitations. The acquisition of CEUS-based candidate biomarkers necessitates an acoustic window to the spinal cord, encompassing the injury center and its periphery. Routine posterior decompression surgery provides such access. In contrast, anterior approaches usually do not offer an optical window large enough for imaging. However, this limitation has become less prominent, given that posterior spinal cord decompression is recommended in the setting of acute tSCI because it allows for more thorough spinal cord decompression and has been associated with improved neurological outcomes (*66*). Another challenge lies in the operator-dependent nature of ultrasound imaging, particularly because patients with tSCI often present during off-hours when dedicated imaging staff is not available. Therefore, training spine surgeons in the acquisition of intraoperative CEUS becomes crucial to enhance the accessibility of this technique. Encouragingly, several prominent spine societies [AOSpine (Arbeitsgemeinschaft für Osteosynthesefragen), NASS (North American Spine Society), and ASIA] have recently endorsed training programs for spine surgeons in intraoperative ultrasound. Another limitation of our study is the single acquisition of posttraumatic CEUS assessments in humans. We acknowledge that tSCI presents a dynamic pathology, and we can only capture the CEUS-derived candidate biomarker at a single time point. In addition, the heterogeneity of human tSCI injury severity, possible differences in injury evolution, and varying durations between injury and CEUS assessment pose further sources of bias in our study. We believe that multiple posttraumatic intraoperative CEUS-derived acquisitions are ethically unjustifiable, because they would prolong the surgical procedure and might endanger the lives of severely injured patients. We have recognized these limitations and developed transcutaneous CEUS in rodents (*67*); however, as of today, transcutaneous CEUS assessments of tSCI have not been demonstrated in humans.

Our study provides encouraging evidence that PAD and SPI are related to tSCI severity and short-term neurological outcomes; however, we acknowledge the need for additional long-term studies of the spinal cord tissue viability after injury to further understand how acute perfusion is related to long-term outcome. The clinical relevance of the proposed CEUS-based biomarkers will require further validation in prospective multicenter studies, particularly to define PAD and SPI thresholds that delineate patients with initially motor-complete injuries who later regain neurological function. Future research is required to determine whether distinct perfusion patterns are associated with spinal cord tissues that are spared versus those that undergo secondary degeneration. Moreover, although the temporal evolution of the PAD in rodent injuries has been studied (*68*), such data are lacking for human tSCI.

In conclusion, CEUS-derived acute perfusion metrics enabled the estimation of injury severity by quantifying vital perfused spinal cord parenchyma at the injury site in both rodent and human tSCI models. The proposed quantitative CEUS-based biomarkers, PAD and SPI, demonstrate substantial prognostic potential in both animal and human tSCI. Future studies should focus on refining standard operating procedures for CEUS imaging acquisition and analysis to further optimize its prognostic capabilities.

MATERIALS AND METHODS

Study design

The objective of the current study was to identify candidate acute, measurable CEUS-derived metrics that correlate with injury severity and functional outcomes in both rodent and human models of tSCI. We conducted a prospective cross-sectional observational study, collecting CEUS data from the acutely injured spinal parenchyma in participants with varying tSCI severity. The study involved calculating potential imaging metrics, including PAD and SPI, to differentiate between irreversibly damaged and potentially viable perfused spinal cord tissue at the injury site. A correlative analysis was then performed to evaluate the relationship between these perfusion metrics and long-term indicators of injury severity and functional recovery. In the preclinical rodent tSCI study, rodents were randomly assigned to mild, moderate, or severe tSCI groups, and researchers were blinded to their status during behavioral assessments and analyses. CEUS parameters, including PAD and SPI, were correlated with functional behavioral tests and spared tissue analysis. All animal studies were approved by the University of Washington Institutional Animal Care and Use Committee (IACUC protocol #4362-01). A power analysis, conducted using G*Power, estimated that about six animals per cohort were needed to detect a statistically significant difference between groups with about 80% power. No animals were excluded from the study.

In a pilot clinical study involving 27 participants, CEUS imaging was performed intraoperatively to assess spinal cord perfusion in patients with acute spinal cord injury who underwent posterior surgical decompression and stabilization. All participants were assigned to the same cohort, and neither participants nor researchers were blinded. Patients were included if they were at least 18 years of age, had a neurological deficit on examination (AIS A to D), and were medically stable to undergo routine posterior spinal decompression and stabilization. Exclusion criteria included penetrating injuries of the spinal cord or nontraumatic spinal cord injuries (table S2). The clinical pilot study was approved by the University of Washington

Institutional Review Board (IRB) (approval #STUDY00003267). All resulting data were included in the analysis, and sample sizes are reported in the figure legends.

Rat spinal cord injury model

All animal procedures were performed in accordance with the guidelines from the Office of Animal Welfare and of the National Institutes of Health and were approved by the University of Washington Institutional Animal Care and Use Committee (IACUC protocol #4362-01). Female Long-Evans rats ($n = 47$, 8 to 12 weeks old; weight, 250 to 300 g, Envigo Labs) were anesthetized using isoflurane (5% to induce and 2.5% to maintain) and shaved, and the area overlying the T6 to T11 vertebrae was cleaned and sterilized. Only female rats were used in this study because males with tSCI can have substantial bladder complications after spinal cord injury. Using sterile techniques, about 2.5-cm longitudinal incision centered over T7 to T10 was made before the subperiostal dissection of the paraspinal muscles. A laminectomy was performed to expose the spinal cord at T8. To produce a contusion type lesion at T8, an Infinite Horizon Device Impactor (IH-0400, Precision Systems and Instrumentation) equipped with a 2.5-mm-diameter probe tip was used. Three different injury severities were produced for this study: mild (100 kDyn; $n = 15$), moderate (150 kDyn; $n = 7$), and severe (200 kDyn; $n = 10$) injuries. Tissue displacement and peak force data were collected, and the actual force recorded was used as an indicator of injury consistency and severity (see table S1). Postsurgical animals were monitored twice daily for dehydration and general health, and manual bladder expression was performed up to 14 days after injury. Spontaneous voiding reflexes returned between 7 and 10 days. Analgesia (buprenorphine, 0.03 mg/kg, sc) was administered every 8 to 12 hours for 48 hours after injury. Antibiotics were administered daily for 5 days to prevent infection (gentamicin, 5 mg/kg; Pfizer).

Ultrasound imaging

The Vantage ultrasound research platform (Verasonics) was used to program multi-angle plane-wave nonlinear Doppler sequences using a 15-MHz linear array transducer (Vermon). The ultrasound probe was placed about 5 mm above the dorsal spinal cord surface over the midline sagittal plane, and warmed sterile ultrasound gel acoustically coupled the transducer to the spinal cord. For each contrast injection, a bolus of 0.1 ml of DEFINITY (Lantheus), activated according to the manufacturer's instruction, was injected intravenously without dilution followed by a 0.2 ml of saline flush. Multi-angle plane-wave transmits acquired at 500- to 2000-Hz pulse repetition frequency were collected. After beam forming and in-phase/quadrature (I/Q) demodulation, ensembles were filtered using a singular value decomposition–based approach to segment flow signals on the basis of relative velocity. This resulted in "vascular flow" and "perfusion" image ensembles, which were analyzed independently (*69*, *70*). Image acquisition was initiated before contrast inflow and proceeded for 30 s after the peak. Short nonlinear ensemble acquisitions (40 frames, amplitude modulation pulsing scheme) were conducted at an interensemble frame rate of 16 Hz. This pulsing scheme eliminated tissue signals, and the use of short, repeated ensembles facilitated the isolation of microcirculatory flow signal from corrupting larger vascular signals using an adaptive spatiotemporal filtering approach. Quantitative parameters were extracted from the resulting time-intensity curve for each spatial voxel to generate a parametric output image. The imaging and postprocessing approaches used for ultrasound localization microscopy have been described in our previous work (*68*). In brief, images were generated using subpixel localization and subsequent interframe tracking of individual circulating microbubbles.

Open-field locomotor test

Animals were acclimated to being handled and to the various pieces of behavioral equipment with which they would be tested for at least 2 weeks before surgery. Baseline behavioral recording for all tests was done 1 week before surgery.

The BBB locomotor rating scale is a sensitive, observer-scored test of hindlimb locomotor function that is commonly used in rodent models after SCI (*71*). Animals were scored according to a standardized score sheet from 0 (no hindlimb movement) to 21 (complete locomotor recovery). Animals were placed into about 100-cm-diameter arena with 19-cm walls (a children's play pool) that has a lightly textured, uniform floor. For 4 min, each animal was permitted to explore the arena as two observers recorded locomotor actions according to the BBB Locomotor Rating Scale (*71*). The observers compared scoring, which was done live, and, if necessary, came to a consensus on the final left and right hindlimb scores. In the present study, the BBB test was repeated every week for 8 weeks. The test was video recorded for reviewing and confirmation of scores if needed.

Ladder walk

The ladder walk test requires no pretraining. This test evaluates sensory-induced motor function of the rodent's limb (*72*). The apparatus consists of two clear plexiglass walls 90 cm long and 15 cm tall, spaced 10 cm apart to create a corridor. A series of 1-mm-diameter stainless steel rungs were intermittently spaced (gaps ranged between 1 and 3 cm) to create a ladder-type floor. The entire apparatus was elevated slightly (about 30 cm) to create a space below for the animal's leg to fall. The home cage was placed at one end of the apparatus. For each trial, the animal was placed at the end opposite to the home cage and walked the length of the apparatus to return to the home cage. Between each successful run, the placement of the rungs was changed to prevent the animals from memorizing a specific rung pattern. The test consisted of 10 trials and was recorded on video. The videos were later reviewed at half speed; the total number of attempted steps and the number of slips or misses (unsuccessful grasps of the rung) were counted for each hindlimb. The percentage of errors was then calculated. In the present study, animals were tested before injury to establish a baseline error percentage and then again at 2 and 8 wpi.

Histological analysis for blood vessel patency

To assess intrinsic spinal cord blood vessel patency, we used fluorescein isothiocyanate–conjugated *Lycopersicon esculentum* agglutinin (tomato) lectin (Sigma-Aldrich). Before tSCI, 0.2 ml (1 mg/ml) was injected by a tail vein. After tSCI, animals received a second injection of Texas Red–labeled lectin. After 30 min, animals were euthanized. A 10-mm-long segment centered over T8 is analyzed for the density of patent microvasculature ($n = 6$). For quantification, a grid of 500 μm^2 was placed over longitudinal photomicrographs using ImageJ. Within each square, distinct microvascular fragments were counted using the multipoint counter tool in ImageJ.

Fluorescent microsphere deposition assay

After thoracic tSCI, rats were positioned in the supine position, and an about-1-mm incision was made on the right side of the neck ($n = 9$).

Blunt dissection was carried out to identify and isolate the carotid artery. Heparinized PE50 tubing was introduced into the artery and advanced to the heart. An inline pressure monitor was used to confirm the tubing location in the right atrium. Silk sutures (4-0) were used to secure the tubing in place. Red or yellow fluorescent microspheres were randomly chosen as either the pre- or postinjury color (Invitrogen, F8842 and F21011). The microspheres were vortexed immediately before injection into the right atrium (0.5 ml). The animals were then prepared for and given the spinal cord injury, as described above, before the postinjury fluorescent microsphere injection of the alternate color (0.5 ml). Animals were euthanized about 30 min after the microsphere injection. Spinal cord tissue (unfixed) was collected. A 10-mm-long spinal cord segment centered at the injury was sectioned 16 μm thick on an imaging cryomicrotome (Barlow Scientific) (*37*). Fluorescent microsphere density was calculated using in-house scripts written for ImageJ and MATLAB (R2017, MathWorks).

Histological analysis for spared tissue

Animals were euthanized at 8 wpi with an overdose of pentobarbital sodium (0.39 g/ml, intraperitoneally; Schering-Plough Animal Health). Animals were fixed by transcardiac perfusion with 200 ml of ice-cold phosphate-buffered saline (pH 7.4) followed by 200 ml of 4% paraformaldehyde (PFA). Spinal cords were harvested and post-fixed in 4% PFA at 4°C for 16 to 18 hours. Spinal cords were mounted and cross-sectionally sectioned using a cryostat (CM1850, Leica Biosystems) at a thickness of 20 μm. Sections were collected, thaw-mounted onto gelatin-coated slides, and stored at −80 °C until use. To perform staining, sections were thawed and fixed with 4% PFA (Macron Chemicals) for 15 min to ensure tissue adherence. Sections then underwent a series of alcohol incubations for dehydration beginning with 4 min in deionized water; followed by 5-min periods in 70, 95, and 100% ethanol; a xylene incubation for 10 min; and then back through the ethanol series. Sections were then incubated for 10 min in an aqueous myelin dye (Eriochrome cyanine R, Fluka) and differentiated for 1 min in 1% ammonium hydroxide (Thermo Fisher Scientific) after washing in water. Sections were then briefly rinsed in water and then incubated in cresyl violet stain (Sigma-Aldrich) for 3 min. After this step, sections were rinsed with deionized water 10 times and then quickly dehydrated in a stepwise manner for 4 min each in 70 and 95% alcohol. The cresyl violet was then briefly differentiated in 250 ml of a 95% alcohol solution containing five drops of glacial acetic acid (Thermo Fisher Scientific). Once differentiation was sufficient, sections continued through a stepwise dehydration process consisting of 5 min each in 95 and 100% ethanol, followed by a final 10-min incubation in xylene. Slides were then cover-slipped using Permount. Cresyl violet–/myelin-stained tissue sections (sampled at 250-μm intervals for 7 mm in length) were imaged using a Zeiss Primo Star microscope with a color camera (Axiocam ERc 5s).

Clinical pilot study

A study protocol outlining patient recruitment, data collection, data storage, and usage was reviewed and approved by the University of Washington IRB (approval #STUDY00003267). Data were collected pseudonymously after written informed consent, in accordance with national law and the 1975 Declaration of Helsinki. Patients who presented to the Harborview Medical Center emergency room within 72 hours after acute tSCI were screened for inclusion in our study. Patients met the inclusion criteria if they were at least 18 years of age, had a neurological deficit on examination (ASIA A to D), and were medically stable to undergo routine posterior spinal decompression and stabilization. Patients were excluded if they had penetrating injuries of the spinal cord or nontraumatic spinal cord injuries (postoperative hematoma and tumor; see table S2). Patients undergoing surgery and CEUS by C.P.H. were recruited between September 2021 and December 2023. The primary end point was the neurological examination at 6 months or death. The main goal of the study was to demonstrate the safety and feasibility of intraoperative CEUS in acute tSCI. All patients were assigned to the same cohort without blinding either the patient or surgeon. No patients were excluded from the analysis.

Intraoperative ultrasound in patients with acute tSCI

Upon completion of a routine posterior decompression and stabilization CEUS was performed by C.P.H. in the operating room at Harborview Medical Center. A Philips EPIQ premium ultrasound system in combination with an intraoperative ultrasound probe (L12-3) was used. First, we obtained B-mode midline sagittal images of the entire rostrocaudal extent of the exposed spinal cord. Before CEUS, the contrast agent (DEFINITY, Lantheus Medical Imaging) was activated in a full 45-s activation cycle using a VIALMIX activator and diluted in saline (1.3 ml of DEFINITY with 8.7 ml of saline) (*73*). Using a peripheral intravenous cannula, a weight-adjusted bolus injection was delivered (10 μl of DEFINITY/kg) as the ultrasound transducer was positioned in a midline sagittal plane. Data acquisition was initiated at the time of contrast injection and continued for up to 3 min after the injection to capture the full dynamic enhancement curve. Patients stayed, on average, 17.6 ± 2.9 days in the hospital, and 19 (70.4%) required inpatient rehabilitation. A return to the operating room was necessary for two patients with surgical site infections and one patient with a postoperative CSF leak.

Analysis of intraoperative ultrasound images

Image analysis was done in a blinded manner. CEUS images were analyzed using the Phillips Q Lab software. First, we used the area outline tool to calculate the size of the PAD on CEUS images. To assess the amount of contrast inflow into the vital tissue at the injury center, we placed a rectangular region of interest (ROI; 3 mm wide and spanning the diameter of the spinal cord; Fig. 5) onto the injury center. Contrast inflow into intact cord tissue was assessed by pacing duplicate ROIs rostral and caudal to the damaged spinal cord areas as determined with B-mode and contrast inflow images. The contrast intensity curve was calculated by the software. The SPI was calculated by normalizing the AUC at the injury center with the average AUC obtained from intact spinal cord rostral and caudal to the injury. The SPI was calculated using the following formula: center perfusion/mean peripheral perfusion.

Statistical analysis

Data were analyzed using Excel (Microsoft), Prism 7 (GraphPad Software), and SPSS (28.0, IBM). Continuous variables are shown as means ± SEM. Before all statistical testing, a Shapiro-Wilk analysis was performed to assess whether the data were normally distributed. To determine significant differences between mild, moderate, and severe rodent tSCI cohorts, we used a one-way analysis of variance (ANOVA) followed by Tukey's post hoc test. A two-way ANOVA was used to test the effects of lesion status and time after injury on behavioral recovery, followed by Bonferroni's multiple comparisons

test. To identify significant differences between patient cohorts, we performed the nonparametric Mann-Whitney *U* test. Pearson's correlation test was used for continuous and normally distributed variables. The coefficient of determination for the Pearson's correlation is denoted as r^2. Correlative analyses for CEUS imaging metrics and AIS grades were carried out using the Spearman's rank correlation test coefficient, r_s. $P < 0.05$ was determined as statistically significant for all analyses. All tabular data are available in data file S1.

Supplementary Materials

The PDF file includes:
Figs. S1 to S4
Tables S1 to S3

Other Supplementary Material for this manuscript includes the following:
Data file S1
MDAR Reproducibility Checklist

REFERENCES AND NOTES

1. C. H. Merritt, M. A. Taylor, C. J. Yelton, S. K. Ray, Economic impact of traumatic spinal cord injuries in the United States. *Neuroimmunol. Neuroinflamm*. **6**, 9 (2019).
2. M. M. Priebe, A. E. Chiodo, W. M. Scelza, S. C. Kirshblum, L. A. Wuermser, C. H. Ho, Spinal cord injury medicine. 6. Economic and societal issues in spinal cord injury. *Arch. Phys. Med. Rehabil.* **88**, S84–S88 (2007).
3. Spinal cord injury (SCI) 2016 facts and figures at a glance. *J. Spinal Cord Med.* **39**, 493–494 (2016).
4. W. Ding, S. Hu, P. Wang, H. Kang, R. Peng, Y. Dong, F. Li, Spinal cord injury: The global incidence, prevalence, and disability from the Global Burden of Disease Study 2019. *Spine (Phila Pa 1976)* **47**, 1532–1540 (2022).
5. A. Ackery, C. Tator, A. Krassioukov, A global perspective on spinal cord injury epidemiology. *J. Neurotrauma* **21**, 1355–1370 (2004).
6. K. Walden, L. M. Belanger, F. Biering-Sorensen, S. P. Burns, E. Echeverria, S. Kirshblum, R. J. Marino, V. K. Noonan, S. E. Park, R. K. Reeves, W. Waring, M. F. Dvorak, Development and validation of a computerized algorithm for International Standards for Neurological Classification of Spinal Cord Injury (ISNCSCI). *Spinal Cord* **54**, 197–203 (2016).
7. S. C. Kirshblum, W. Waring, F. Biering-Sorensen, S. P. Burns, M. Johansen, M. Schmidt-Read, W. Donovan, D. Graves, A. Jha, L. Jones, M. J. Mulcahey, A. Krassioukov, Reference for the 2011 revision of the International Standards for Neurological Classification of Spinal Cord Injury. *J. Spinal Cord Med.* **34**, 547–554 (2011).
8. J. C. Furlan, V. Noonan, D. W. Cadotte, M. G. Fehlings, Timing of decompressive surgery of spinal cord after traumatic spinal cord injury: An evidence-based examination of pre-clinical and clinical studies. *J. Neurotrauma* **28**, 1371–1399 (2011).
9. G. Savic, E. M. Bergstrom, H. L. Frankel, M. A. Jamous, P. W. Jones, Inter-rater reliability of motor and sensory examinations performed according to American Spinal Injury Association standards. *Spinal Cord* **45**, 444–451 (2007).
10. R. J. Marino, L. Jones, S. Kirshblum, J. Tal, A. Dasgupta, Reliability and repeatability of the motor and sensory examination of the international standards for neurological classification of spinal cord injury. *J. Spinal Cord Med.* **31**, 166–170 (2008).
11. S. Kirshblum, B. Snider, F. Eren, J. Guest, Characterizing natural recovery after traumatic spinal cord injury. *J. Neurotrauma* **38**, 1267–1284 (2021).
12. R. L. Waters, R. H. Adkins, J. S. Yakura, I. Sie, Motor and sensory recovery following incomplete tetraplegia. *Arch. Phys. Med. Rehabil.* **75**, 306–311 (1994).
13. R. L. Waters, R. H. Adkins, J. S. Yakura, I. Sie, Motor and sensory recovery following incomplete paraplegia. *Arch. Phys. Med. Rehabil.* **75**, 67–72 (1994).
14. R. L. Waters, R. H. Adkins, J. S. Yakura, I. Sie, Motor and sensory recovery following complete tetraplegia. *Arch. Phys. Med. Rehabil.* **74**, 242–247 (1993).
15. R. L. Waters, J. S. Yakura, R. H. Adkins, I. Sie, Recovery following complete paraplegia. *Arch. Phys. Med. Rehabil.* **73**, 784–789 (1992).
16. M. G. Fehlings, A. Moghaddamjou, J. S. Harrop, R. Stanford, J. Ball, B. Aarabi, B. J. C. Freeman, P. M. Arnold, J. D. Guest, S. N. Kurpad, J. M. Schuster, A. Nassr, K. M. Schmitt, J. R. Wilson, D. S. Brodke, F. U. Ahmad, A. Yee, W. Z. Ray, N. P. Brooks, J. Wilson, D. S. Chow, E. G. Toups, B. Kopjar, Safety and efficacy of Riluzole in Acute Spinal Cord Injury Study (RISCIS): A multi-center, randomized, placebo-controlled, double-blinded trial. *J. Neurotrauma* **40**, 1878–1888 (2023).
17. M. B. Bracken, M. J. Shepard, T. R. Holford, L. Leo-Summers, E. F. Aldrich, M. Fazl, M. Fehlings, D. L. Herr, P. W. Hitchon, L. F. Marshall, R. P. Nockels, V. Pascale, P. L. Perot Jr., J. Piepmeier, V. K. Sonntag, F. Wagner, J. E. Wilberger, H. R. Winn, W. Young, Administration of methylprednisolone for 24 or 48 hours or tirilazad mesylate for 48 hours in the treatment of acute spinal cord injury. Results of the Third National Acute Spinal Cord Injury Randomized Controlled Trial. National Acute Spinal Cord Injury Study. *JAMA* **277**, 1597–1604 (1997).
18. F. H. Geisler, W. P. Coleman, G. Grieco, D. Poonian, Sygen Study Group, The Sygen multicenter acute spinal cord injury study. *Spine (Phila Pa 1976)* **26**, S87–S98 (2001).
19. J. H. Badhiwala, J. R. Wilson, C. D. Witiw, J. S. Harrop, A. R. Vaccaro, B. Aarabi, R. G. Grossman, F. H. Geisler, M. G. Fehlings, The influence of timing of surgical decompression for acute spinal cord injury: A pooled analysis of individual patient data. *Lancet Neurol.* **20**, 117–126 (2021).
20. W. K. Hsu, Transient quadriparesis and cervical neuropraxia in elite athletes. *Clin. Sports Med.* **40**, 463–470 (2021).
21. M. G. Fehlings, L. A. Tetreault, L. Hachem, N. Evaniew, M. Ganau, S. L. McKenna, C. J. Neal, N. Nagoshi, V. Rahimi-Movaghar, B. Aarabi, C. P. Hofstetter, V. T. Wengel, H. Nakashima, A. R. Martin, S. Kirshblum, R. Rodrigues Pinto, R. A. W. Marco, J. R. Wilson, D. E. Kahn, V. F. J. Newcombe, C. M. Zipser, S. Douglas, S. N. Kurpad, Y. Lu, R. Saigal, U. Samadani, P. M. Arnold, G. W. J. Hawryluk, A. C. Skelly, B. K. Kwon, An update of a clinical practice guideline for the management of patients with acute spinal cord injury: Recommendations on the role and timing of decompressive surgery. *Global Spine J.* **14**, 174S–186S (2024).
22. N. Evaniew, B. Sharifi, Z. Waheed, N. Fallah, T. Ailon, N. Dea, S. Paquette, R. Charest-Morin, J. Street, C. G. Fisher, M. F. Dvorak, V. K. Noonan, C. S. Rivers, B. K. Kwon, The influence of neurological examination timing within hours after acute traumatic spinal cord injuries: An observational study. *Spinal Cord* **58**, 247–254 (2020).
23. Z. Z. Khaing, L. N. Cates, J. Hyde, D. M. DeWees, R. Hammond, M. Bruce, C. P. Hofstetter, Contrast-enhanced ultrasound for assessment of local hemodynamic changes following a rodent contusion spinal cord injury. *Mil. Med.* **185**, 470–475 (2020).
24. E. Le, B. Aarabi, D. S. Hersh, K. Shanmuganathan, C. Diaz, J. Massetti, N. Akhtar-Danesh, Predictors of intramedullary lesion expansion rate on MR images of patients with subaxial spinal cord injury. *J. Neurosurg. Spine* **22**, 611–621 (2015).
25. G. J. Herbison, S. A. Zerby, M. E. Cohen, R. J. Marino, J. F. Ditunno Jr., Motor power differences within the first two weeks post-SCI in cervical spinal cord-injured quadriplegic subjects. *J. Neurotrauma* **9**, 373–380 (1992).
26. P. J. Brown, R. J. Marino, G. J. Herbison, J. F. Ditunno Jr., The 72-hour examination as a predictor of recovery in motor complete quadriplegia. *Arch. Phys. Med. Rehabil.* **72**, 546–548 (1991).
27. A. S. Burns, B. S. Lee, J. F. Ditunno Jr., A. Tessler, Patient selection for clinical trials: the reliability of the early spinal cord injury examination. *J. Neurotrauma* **20**, 477–482 (2003).
28. B. K. Kwon, F. Streijger, N. Fallah, V. K. Noonan, L. M. Belanger, L. Ritchie, S. J. Paquette, T. Ailon, M. C. Boyd, J. Street, C. G. Fisher, M. F. Dvorak, Cerebrospinal fluid biomarkers to stratify injury severity and predict outcome in human traumatic spinal cord injury. *J. Neurotrauma* **34**, 567–580 (2017).
29. B. Aarabi, C. A. Sansur, D. M. Ibrahimi, J. M. Simard, D. S. Hersh, E. Le, C. Diaz, J. Massetti, N. Akhtar-Danesh, Intramedullary lesion length on postoperative magnetic resonance imaging is a strong predictor of asia impairment scale grade conversion following decompressive surgery in cervical spinal cord injury. *Neurosurgery* **80**, 610–620 (2017).
30. J. Haefeli, M. C. Mabray, W. D. Whetstone, S. S. Dhall, J. Z. Pan, P. Upadhyayula, G. T. Manley, J. C. Bresnahan, M. S. Beattie, A. R. Ferguson, J. F. Talbott, Multivariate analysis of MRI biomarkers for predicting neurologic impairment in cervical spinal cord injury. *AJNR Am. J. Neuroradiol.* **38**, 648–655 (2017).
31. F. Miyanji, J. C. Furlan, B. Aarabi, P. M. Arnold, M. G. Fehlings, Acute cervical traumatic spinal cord injury: MR imaging findings correlated with neurologic outcome--prospective study with 100 consecutive patients. *Radiology* **243**, 820–827 (2007).
32. M. Soubeyrand, A. Badner, R. Vawda, Y. S. Chung, M. G. Fehlings, Very high resolution ultrasound imaging for real-time quantitative visualization of vascular disruption after spinal cord injury. *J. Neurotrauma* **31**, 1767–1775 (2014).
33. Z. Z. Khaing, L. N. Cates, D. M. DeWees, A. Hannah, P. Mourad, M. Bruce, C. P. Hofstetter, Contrast-enhanced ultrasound to visualize hemodynamic changes after rodent spinal cord injury. *J. Neurosurg. Spine* **29**, 306–313 (2018).
34. J. S. Harmon, Z. Z. Khaing, J. E. Hyde, C. P. Hofstetter, C. Tremblay-Darveau, M. F. Bruce, Quantitative tissue perfusion imaging using nonlinear ultrasound localization microscopy. *Sci. Rep.* **12**, 21943 (2022).
35. M. Bruce, D. DeWees, J. Harmon, L. Cates, Z. Z. Khaing, C. P. Hofstetter, Blood flow changes associated with spinal cord injury assessed by non-linear doppler contrast-enhanced ultrasound. *Ultrasound Med. Biol.* **48**, 1410–1419 (2022).
36. C. H. Tator, M. G. Fehlings, Review of the secondary injury theory of acute spinal cord trauma with emphasis on vascular mechanisms. *J. Neurosurg.* **75**, 15–26 (1991).
37. S. L. Bernard, J. R. Ewen, C. H. Barlow, J. J. Kelly, S. McKinney, D. A. Frazer, R. W. Glenny, High spatial resolution measurements of organ blood flow in small laboratory animals. *Am. J. Physiol. Heart Circ. Physiol.* **279**, H2043–H2052 (2000).
38. D. J. Fairholm, I. M. Turnbull, Microangiographic study of experimental spinal cord injuries. *J. Neurosurg.* **35**, 277–286 (1971).

39. M. C. Wallace, C. H. Tator, Spinal cord blood flow measured with microspheres following spinal cord injury in the rat. *Can. J. Neurol. Sci.* **13**, 91–96 (1986).
40. A. N. Sandler, C. H. Tator, Effect of acute spinal cord compression injury on regional spinal cord blood flow in primates. *J. Neurosurg.* **45**, 660–676 (1976).
41. A. S. Rivlin, C. H. Tator, Regional spinal cord blood flow in rats after severe cord trauma. *J. Neurosurg.* **49**, 844–853 (1978).
42. I. Piper, A. Guha, C. H. Tator, W. Gentles, A microcomputer system for on-line collection of blood flow and related physiological data. *Comput. Biol. Med.* **17**, 279–291 (1987).
43. M. G. Fehlings, C. H. Tator, R. D. Linden, The relationships among the severity of spinal cord injury, motor and somatosensory evoked potentials and spinal cord blood flow. *Electroencephalogr. Clin. Neurophysiol.* **74**, 241–259 (1989).
44. M. F. Dvorak, V. K. Noonan, N. Fallah, C. G. Fisher, C. S. Rivers, H. Ahn, E. C. Tsai, A. G. Linassi, S. D. Christie, N. Attabib, R. J. Hurlbert, D. R. Fourney, M. G. Johnson, M. G. Fehlings, B. Drew, C. S. Bailey, J. Paquet, S. Parent, A. Townson, C. Ho, B. C. Craven, D. Gagnon, D. Tsui, R. Fox, J. M. Mac-Thiong, B. K. Kwon, Minimizing errors in acute traumatic spinal cord injury trials by acknowledging the heterogeneity of spinal cord anatomy and injury severity: An observational Canadian cohort analysis. *J. Neurotrauma* **31**, 1540–1547 (2014).
45. S. W. Scheff, A. G. Rabchevsky, I. Fugaccia, J. A. Main, J. E. Lumpp Jr., Experimental modeling of spinal cord injury: Characterization of a force-defined injury device. *J. Neurotrauma* **20**, 179–193 (2003).
46. A. D. Levi, J. M. Schwab, A critical reappraisal of corticospinal tract somatotopy and its role in traumatic cervical spinal cord syndromes. *J. Neurosurg. Spine* **36**, 653–659 (2022).
47. R. Blecher, E. Yilmaz, B. Ishak, A. von Glinski, M. Moisi, R. J. Oskouian, J. Dettori, M. Kramer, M. Drexler, J. R. Chapman, Uptrend of cervical and sacral fractures underlie increase in spinal fractures in the elderly, 2003-2017: Analysis of a state-wide population database. *Eur. Spine J.* **29**, 2543–2549 (2020).
48. M. J. Gallagher, F. R. A. Hogg, A. Zoumprouli, M. C. Papadopoulos, S. Saadoun, Spinal cord blood flow in patients with acute spinal cord injuries. *J. Neurotrauma* **36**, 919–929 (2019).
49. G. Dwivedi, L. Flaman, B. Alaybeyoglu, A. Struglics, E. H. Frank, S. Chubinskya, S. B. Trippel, V. Rosen, M. Cirit, A. J. Grodzinsky, Inflammatory cytokines and mechanical injury induce post-traumatic osteoarthritis-like changes in a human cartilage-bone-synovium microphysiological system. *Arthritis Res. Ther.* **24**, 198 (2022).
50. R. M. Black, L. L. Flaman, K. Lindblom, S. Chubinskaya, A. J. Grodzinsky, P. Onnerfjord, Tissue catabolism and donor-specific dexamethasone response in a human osteochondral model of post-traumatic osteoarthritis. *Arthritis Res. Ther.* **24**, 137 (2022).
51. G. D. Carlson, Y. Minato, A. Okada, C. D. Gorden, K. E. Warden, J. M. Barbeau, C. L. Biro, E. Bahnuik, H. H. Bohlman, J. C. Lamanna, Early time-dependent decompression for spinal cord injury: Vascular mechanisms of recovery. *J. Neurotrauma* **14**, 951–962 (1997).
52. S. Mattucci, J. Speidel, J. Liu, B. K. Kwon, W. Tetzlaff, T. R. Oxland, Basic biomechanics of spinal cord injury—How injuries happen in people and how animal models have informed our understanding. *Clin. Biomech. (Bristol, Avon)* **64**, 58–68 (2019).
53. B. K. Kwon, A. M. Stammers, L. M. Belanger, A. Bernardo, D. Chan, C. M. Bishop, G. P. Slobogean, H. Zhang, H. Umedaly, M. Giffin, J. Street, M. C. Boyd, S. J. Paquette, C. G. Fisher, M. F. Dvorak, Cerebrospinal fluid inflammatory cytokines and biomarkers of injury severity in acute human spinal cord injury. *J. Neurotrauma* **27**, 669–682 (2010).
54. M. H. Pouw, B. K. Kwon, M. M. Verbeek, P. E. Vos, A. van Kampen, C. G. Fisher, J. Street, S. J. Paquette, M. F. Dvorak, M. C. Boyd, A. J. Hosman, H. van de Meent, Structural biomarkers in the cerebrospinal fluid within 24 h after a traumatic spinal cord injury: A descriptive analysis of 16 subjects. *Spinal Cord* **52**, 428–433 (2014).
55. R. Ahadi, F. Khodagholi, A. Daneshi, A. Vafaei, A. A. Mafi, M. Jorjani, Diagnostic value of serum levels of GFAP, pNF-H, and NSE compared with clinical findings in severity assessment of human traumatic spinal cord injury. *Spine (Phila Pa 1976)* **40**, E823–E830 (2015).
56. J. F. Talbott, W. D. Whetstone, W. J. Readdy, A. R. Ferguson, J. C. Bresnahan, R. Saigal, G. W. Hawryluk, M. S. Beattie, M. C. Mabray, J. Z. Pan, G. T. Manley, S. S. Dhall, The Brain and Spinal Injury Center score: A novel, simple, and reproducible method for assessing the severity of acute cervical spinal cord injury with axial T2-weighted MRI findings. *J. Neurosurg. Spine* **23**, 495–504 (2015).
57. M. Seif, A. Curt, A. J. Thompson, P. Grabher, N. Weiskopf, P. Freund, Quantitative MRI of rostral spinal cord and brain regions is predictive of functional recovery in acute spinal cord injury. *Neuroimage Clin.* **20**, 556–563 (2018).
58. J. Hou, Z. Xiang, R. Yan, M. Zhao, Y. Wu, J. Zhong, L. Guo, H. Li, J. Wang, J. Wu, T. Sun, H. Liu, Motor recovery at 6 months after admission is related to structural and functional reorganization of the spine and brain in patients with spinal cord injury. *Hum. Brain Mapp.* **37**, 2195–2209 (2016).
59. G. David, M. Seif, E. Huber, M. Hupp, J. Rosner, V. Dietz, N. Weiskopf, S. Mohammadi, P. Freund, In vivo evidence of remote neural degeneration in the lumbar enlargement after cervical injury. *Neurology* **92**, e1367–e1377 (2019).
60. E. Huber, G. David, A. J. Thompson, N. Weiskopf, S. Mohammadi, P. Freund, Dorsal and ventral horn atrophy is associated with clinical outcome after spinal cord injury. *Neurology* **90**, e1510–e1522 (2018).
61. M. J. Mulcahey, A. Samdani, J. Gaughan, N. Barakat, S. Faro, R. R. Betz, J. Finsterbusch, F. B. Mohamed, Diffusion tensor imaging in pediatric spinal cord injury: Preliminary examination of reliability and clinical correlation. *Spine (Phila Pa 1976)* **37**, E797–E803 (2012).
62. S. Cheran, K. Shanmuganathan, J. Zhuo, S. E. Mirvis, B. Aarabi, M. T. Alexander, R. P. Gullapalli, Correlation of MR diffusion tensor imaging parameters with ASIA motor scores in hemorrhagic and nonhemorrhagic acute spinal cord injury. *J. Neurotrauma* **28**, 1881–1892 (2011).
63. S. A. Murphy, R. Furger, S. N. Kurpad, V. E. Arpinar, A. Nencka, K. Koch, M. D. Budde, Filtered diffusion-weighted MRI of the human cervical spinal cord: Feasibility and application to traumatic spinal cord injury. *AJNR Am. J. Neuroradiol.* **42**, 2101–2106 (2021).
64. Y. Chang, T. D. Jung, D. S. Yoo, J. K. Hyun, Diffusion tensor imaging and fiber tractography of patients with cervical spinal cord injury. *J. Neurotrauma* **27**, 2033–2040 (2010).
65. F. H. Brennan, G. J. Cowin, N. D. Kurniawan, M. J. Ruitenberg, Longitudinal assessment of white matter pathology in the injured mouse spinal cord through ultra-high field (16.4 T) in vivo diffusion tensor imaging. *Neuroimage* **82**, 574–585 (2013).
66. B. Aarabi, J. Olexa, T. Chryssikos, S. M. Galvagno, D. S. Hersh, A. Wessell, C. Sansur, G. Schwartzbauer, K. Crandall, K. Shanmuganathan, J. M. Simard, H. Mushlin, M. Kole, E. Le, N. Pratt, G. Cannarsa, C. D. Lomangino, M. Scarboro, C. Aresco, B. Curry, Extent of spinal cord decompression in motor complete (American Spinal Injury Association Impairment Scale Grades A and B) traumatic spinal cord injury patients: Post-operative magnetic resonance imaging analysis of standard operative approaches. *J. Neurotrauma* **36**, 862–876 (2019).
67. Z. Z. Khaing, L. N. Cates, J. E. Hyde, R. Hammond, M. Bruce, C. P. Hofstetter, Transcutaneous contrast-enhanced ultrasound imaging of the posttraumatic spinal cord. *Spinal Cord* **58**, 695–704 (2020).
68. J. N. Harmon, J. E. Hyde, D. E. Jensen, E. C. D'cessare, A. A. Odarenko, M. F. Bruce, Z. Z. Khaing, Quantifying injury expansion in the cervical spinal cord with intravital ultrafast contrast-enhanced ultrasound imaging. *Exp. Neurol.* **374**, 114681 (2024).
69. M. Bruce, A. Hannah, R. Hammond, Z. Z. Khaing, C. Tremblay-Darveau, P. N. Burns, C. P. Hofstetter, High frequency nonlinear Doppler contrast-enhanced ultrasound imaging of blood flow. *IEEE Trans. Ultrason. Ferroelectr. Freq. Control* **67**, 1776–1784 (2020).
70. C. Tremblay-Darveau, R. Williams, L. Milot, M. Bruce, P. N. Burns, Visualizing the tumor microvasculature with a nonlinear plane-wave doppler imaging scheme based on amplitude modulation. *IEEE Trans. Med. Imaging* **35**, 699–709 (2016).
71. D. M. Basso, M. S. Beattie, J. C. Bresnahan, A sensitive and reliable locomotor rating scale for open field testing in rats. *J. Neurotrauma* **12**, 1–21 (1995).
72. G. A. Metz, I. Q. Whishaw, The ladder rung walking task: A scoring system and its practical application. *J. Vis. Exp.* **12**, 1204 (2009).
73. L. L. Kusnetzky, A. Khalid, T. M. Khumri, T. G. Moe, P. G. Jones, M. L. Main, Acute mortality in hospitalized patients undergoing echocardiography with and without an ultrasound contrast agent: Results in 18,671 consecutive studies. *J. Am. Coll. Cardiol.* **51**, 1704–1706 (2008).

Acknowledgments

Funding: This work is supported partly by the Department of Neurological Surgery, the Royalty Research Fund at the University of Washington, the Washington State Spinal Cord Injury Fund, the Raisbeck family foundation grant from Lantheus that provided microbubbles for our rodent studies (to C.P.H. and Z.Z.K.), the Craig Neilsen Foundation (#546901 to C.P.H.), and the Department of Defense (CDMRP TRA-W81XWH-18-1-0753 to C.P.H.). We acknowledge the Philips for providing the EPIQ ultrasound machine. **Author contributions:** Z.Z.K., C.P.H., M.K., R.W.G., and M.B. were involved in the conception and design of the work. Z.Z.K., J.L., J.N.H., L.N.C., J.E.H., M.K., C.P.H., and M.B. conducted the rodent studies. J.L. and J.E.H. conducted the behavioral analysis. C.P.H., J.L., and S.S. conducted the clinical pilot study. C.P.H. performed the surgery and collected ultrasound images. C.P.H. and M.B. performed analysis related to the clinical images. Z.Z.K., J.L., J.E.H., and C.P.H. drafted the manuscript and participated in revisions. **Competing interests:** C.P.H. teaches and consults for Joimax, J&J, Globus, and Kuros. Z.Z.K. has performed consulting work with Applied Research Associates and for L. Hulbert at the Kansas State University. M.B. consults for Verasonics Inc. All other authors declare that they have no competing interests. **Data and materials availability:** All data associated with this study are present in the paper or the Supplementary Materials.

Submitted 12 December 2023
Resubmitted 25 April 2024
Accepted 28 August 2024
Published 18 September 2024
10.1126/scitranslmed.adn4970